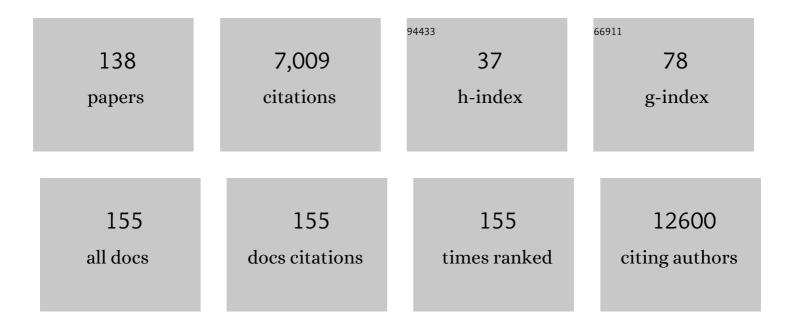
List of Publications by Year in descending order

Source: https://exaly.com/author-pdf/2562878/publications.pdf Version: 2024-02-01



FEI SUM

#	Article	IF	CITATIONS
1	Inhibition of SARS-CoV-2 (previously 2019-nCoV)Âinfection by a highly potent pan-coronavirus fusion inhibitor targeting its spike protein that harbors a high capacity to mediate membrane fusion. Cell Research, 2020, 30, 343-355.	12.0	1,083
2	Secreted Monocytic miR-150 Enhances Targeted Endothelial Cell Migration. Molecular Cell, 2010, 39, 133-144.	9.7	1,059
3	Crystal Structure of Mitochondrial Respiratory Membrane Protein Complex II. Cell, 2005, 121, 1043-1057.	28.9	689
4	Insights into SARS-CoV transcription and replication from the structure of the nsp7–nsp8 hexadecamer. Nature Structural and Molecular Biology, 2005, 12, 980-986.	8.2	255
5	The Intra-S Phase Checkpoint Targets Dna2 to Prevent Stalled Replication Forks from Reversing. Cell, 2012, 149, 1221-1232.	28.9	149
6	An electron transfer path connects subunits of a mycobacterial respiratory supercomplex. Science, 2018, 362, .	12.6	117
7	Structural basis of G _s and G _i recognition by the human glucagon receptor. Science, 2020, 367, 1346-1352.	12.6	117
8	Acyl-CoA Dehydrogenase Drives Heat Adaptation by Sequestering Fatty Acids. Cell, 2015, 161, 1152-1163.	28.9	105
9	Coexistence of ribbon and helical fibrils originating from hIAPP _{20–29} revealed by quantitative nanomechanical atomic force microscopy. Proceedings of the National Academy of Sciences of the United States of America, 2013, 110, 2798-2803.	7.1	104
10	Molecular insights into the enzyme promiscuity of an aromatic prenyltransferase. Nature Chemical Biology, 2017, 13, 226-234.	8.0	100
11	Dodecamer Structure of Severe Acute Respiratory Syndrome Coronavirus Nonstructural Protein nsp10. Journal of Virology, 2006, 80, 7902-7908.	3.4	95
12	A single-cell transcriptomic landscape of primate arterial aging. Nature Communications, 2020, 11, 2202.	12.8	95
13	Atomic Model of Rabbit Hemorrhagic Disease Virus by Cryo-Electron Microscopy and Crystallography. PLoS Pathogens, 2013, 9, e1003132.	4.7	94
14	Three-dimensional super-resolution protein localization correlated with vitrified cellular context. Scientific Reports, 2015, 5, 13017.	3.3	94
15	New Antiviral Target Revealed by the Hexameric Structure of Mouse Hepatitis Virus Nonstructural Protein nsp15. Journal of Virology, 2006, 80, 7909-7917.	3.4	85
16	Structural insights into Ca2+-activated long-range allosteric channel gating of RyR1. Cell Research, 2016, 26, 977-994.	12.0	84
17	Crystal structure of E. coli lipoprotein diacylglyceryl transferase. Nature Communications, 2016, 7, 10198.	12.8	81
18	Structural insights into the peroxidase activity and inactivation of human peroxiredoxin 4. Biochemical Journal, 2012, 441, 113-118.	3.7	77

#	Article	IF	CITATIONS
19	ICON: 3D reconstruction with â€~missing-information' restoration in biological electron tomography. Journal of Structural Biology, 2016, 195, 100-112.	2.8	75
20	The p53-induced Gene Ei24 Is an Essential Component of the Basal Autophagy Pathway. Journal of Biological Chemistry, 2012, 287, 42053-42063.	3.4	68
21	Crystal structure of human ERp44 shows a dynamic functional modulation by its carboxyâ€ŧerminal tail. EMBO Reports, 2008, 9, 642-647.	4.5	66
22	Structures of human mGlu2 and mGlu7 homo- and heterodimers. Nature, 2021, 594, 589-593.	27.8	66
23	Atomic model of a cypovirus built from cryo-EM structure provides insight into the mechanism of mRNA capping. Proceedings of the National Academy of Sciences of the United States of America, 2011, 108, 1373-1378.	7.1	65
24	Synthetic Multienzyme Complexes, Catalytic Nanomachineries for Cascade Biosynthesis <i>In Vivo</i> . ACS Nano, 2019, 13, 9895-9906.	14.6	65
25	Five mutations in N-terminus confer thermostability on mesophilic xylanase. Biochemical and Biophysical Research Communications, 2010, 395, 200-206.	2.1	59
26	Cryo-EM structure of the RC-LH core complex from an early branching photosynthetic prokaryote. Nature Communications, 2018, 9, 1568.	12.8	59
27	The Role and Structure of the Carboxyl-terminal Domain of the Human Voltage-gated Proton Channel Hv1. Journal of Biological Chemistry, 2010, 285, 12047-12054.	3.4	56
28	Cryo-EM structure of a transcribing cypovirus. Proceedings of the National Academy of Sciences of the United States of America, 2012, 109, 6118-6123.	7.1	52
29	Molecular insights into the membrane-associated phosphatidylinositol 4-kinase IIα. Nature Communications, 2014, 5, 3552.	12.8	52
30	Crystal Structure of Tabtoxin Resistance Protein Complexed with Acetyl Coenzyme A Reveals the Mechanism for β-Lactam Acetylation. Journal of Molecular Biology, 2003, 325, 1019-1030.	4.2	46
31	Crystal structure and mutagenic analysis of GDOsp, a gentisate 1,2â€dioxygenase from <i>Silicibacter Pomeroyi</i> . Protein Science, 2008, 17, 1362-1373.	7.6	46
32	Thiabendazole inhibits ubiquinone reduction activity of mitochondrial respiratory complex II via a water molecule mediated binding feature. Protein and Cell, 2011, 2, 531-542.	11.0	45
33	Three-dimensional reconstruction using an adaptive simultaneous algebraic reconstruction technique in electron tomography. Journal of Structural Biology, 2011, 175, 277-287.	2.8	43
34	Minireview of progress in the structural study of SARS-CoV-2 proteins. Current Research in Microbial Sciences, 2020, 1, 53-61.	2.3	43
35	An improved cryo-FIB method for fabrication of frozen hydrated lamella. Journal of Structural Biology, 2016, 194, 218-223.	2.8	42
36	Atlastin-1 regulates morphology and function of endoplasmic reticulum in dendrites. Nature Communications, 2019, 10, 568.	12.8	41

#	Article	IF	CITATIONS
37	Novel cleavage sites identified in SARS-CoV-2 spike protein reveal mechanism for cathepsin L-facilitated viral infection and treatment strategies. Cell Discovery, 2022, 8, .	6.7	40
38	Autotransporter passenger domain secretion requires a hydrophobic cavity at the extracellular entrance of the Î ² -domain pore. Biochemical Journal, 2011, 435, 577-587.	3.7	39
39	A novel fully automatic scheme for fiducial marker-based alignment in electron tomography. Journal of Structural Biology, 2015, 192, 403-417.	2.8	39
40	Crystal Structure of Group II Chaperonin in the Open State. Structure, 2010, 18, 1270-1279.	3.3	38
41	In situ protein micro-crystal fabrication by cryo-FIB for electron diffraction. Biophysics Reports, 2018, 4, 339-347.	0.8	38
42	Structural and functional basis for pan-CoV fusion inhibitors against SARS-CoV-2 and its variants with preclinical evaluation. Signal Transduction and Targeted Therapy, 2021, 6, 288.	17.1	38
43	Cryo-EM structures of S-OPA1 reveal its interactions with membrane and changes upon nucleotide binding. ELife, 2020, 9, .	6.0	38
44	Design and Structure-Based Study of New Potential FKBP12 Inhibitors. Biophysical Journal, 2003, 85, 3194-3201.	0.5	37
45	Revealing various coupling of electron transfer and proton pumping in mitochondrial respiratory chain. Current Opinion in Structural Biology, 2013, 23, 526-538.	5.7	35
46	A marker-free automatic alignment method based on scale-invariant features. Journal of Structural Biology, 2014, 186, 167-180.	2.8	35
47	Structural Insights into the Intrinsic Self-Assembly of Par-3 N-Terminal Domain. Structure, 2013, 21, 997-1006.	3.3	34
48	Amorphous nickel titanium alloy film: A new choice for cryo electron microscopy sample preparation. Progress in Biophysics and Molecular Biology, 2020, 156, 3-13.	2.9	33
49	Structural Basis for the Specific Recognition of RET by the Dok1 Phosphotyrosine Binding Domain. Journal of Biological Chemistry, 2004, 279, 4962-4969.	3.4	32
50	A PH Domain in ACAP1 Possesses Key Features of the BAR Domain in Promoting Membrane Curvature. Developmental Cell, 2014, 31, 73-86.	7.0	32
51	Identification of SERPINB1 As a Physiological Inhibitor of Human Granzyme H. Journal of Immunology, 2013, 190, 1319-1330.	0.8	31
52	Cryo-EM structures of two bovine adenovirus type 3 intermediates. Virology, 2014, 450-451, 174-181.	2.4	31
53	Crystal structure of E. coli apolipoprotein N-acyl transferase. Nature Communications, 2017, 8, 15948.	12.8	31
54	Nanometer-resolution in situ structure of the SARS-CoV-2 postfusion spike protein. Proceedings of the United States of America, 2021, 118, .	7.1	30

#	Article	IF	CITATIONS
55	The Crystal Structure of Human Isopentenyl Diphosphate Isomerase at 1.7ÂÃ Resolution Reveals its Catalytic Mechanism in Isoprenoid Biosynthesis. Journal of Molecular Biology, 2007, 366, 1447-1458.	4.2	29
56	Large scale three-dimensional reconstruction of an entire Caenorhabditis elegans larva using AutoCUTS-SEM. Journal of Structural Biology, 2017, 200, 87-96.	2.8	28
57	Cryo-electron microscopy reconstructions of two types of wild rabbit hemorrhagic disease viruses characterized the structural features of Lagovirus. Protein and Cell, 2010, 1, 48-58.	11.0	27
58	High-vacuum optical platform for cryo-CLEM (HOPE): A new solution for non-integrated multiscale correlative light and electron microscopy. Journal of Structural Biology, 2018, 201, 63-75.	2.8	27
59	FIRT: Filtered iterative reconstruction technique with information restoration. Journal of Structural Biology, 2016, 195, 49-61.	2.8	26
60	Structural Basis for Proteolytic Specificity of the Human Apoptosis-Inducing Granzyme M. Journal of Immunology, 2009, 183, 421-429.	0.8	25
61	Mechanistic Insights into Regulated Cargo Binding by ACAP1 Protein. Journal of Biological Chemistry, 2012, 287, 28675-28685.	3.4	25
62	AuTom: A novel automatic platform for electron tomography reconstruction. Journal of Structural Biology, 2017, 199, 196-208.	2.8	25
63	NLRP6 self-assembles into a linear molecular platform following LPS binding and ATP stimulation. Scientific Reports, 2020, 10, 198.	3.3	23
64	8 Ã structure of the outer rings of the Xenopus laevis nuclear pore complex obtained by cryo-EM and Al. Protein and Cell, 2022, 13, 760-777.	11.0	23
65	A cryo-electron microscopy support film formed by 2D crystals of hydrophobin HFBI. Nature Communications, 2021, 12, 7257.	12.8	23
66	Thermodynamics of voltage-gated ion channels. Biophysics Reports, 2018, 4, 300-319.	0.8	22
67	Three-dimensional reconstruction of Picea wilsonii Mast. pollen grains using automated electron microscopy. Science China Life Sciences, 2020, 63, 171-179.	4.9	20
68	Crystal Structure of a Novel Esterase Rv0045c from Mycobacterium tuberculosis. PLoS ONE, 2011, 6, e20506.	2.5	20
69	Structural Insights into the Substrate Specificity of Human Granzyme H: The Functional Roles of a Novel RKR Motif. Journal of Immunology, 2012, 188, 765-773.	0.8	19
70	A novel mitochondrial carrier protein Mme1 acts as a yeast mitochondrial magnesium exporter. Biochimica Et Biophysica Acta - Molecular Cell Research, 2015, 1853, 724-732.	4.1	19
71	Structure Based Hyperthermostability of Archaeal Histone HPhA from Pyrococcus horikoshii. Journal of Molecular Biology, 2003, 325, 1031-1037.	4.2	18
72	Changes in the quaternary structure and function of MjHSP16.5 attributable to deletion of the IXI motif and introduction of the substitution, R107G, in the <i>î±</i> -crystallin domain. Philosophical Transactions of the Royal Society B: Biological Sciences, 2013, 368, 20120327.	4.0	18

#	Article	IF	CITATIONS
73	Cryo-EM Structure of Actin Filaments from <i>Zea mays</i> Pollen. Plant Cell, 2019, 31, 2855-2867.	6.6	18
74	MicroRNA-124 reduces caveolar density by targeting caveolin-1 in porcine kidney epithelial PK15 cells. Molecular and Cellular Biochemistry, 2013, 384, 213-219.	3.1	17
75	Molecular Details of the PH Domain of ACAP1 ^{BAR-PH} Protein Binding to PIP-Containing Membrane. Journal of Physical Chemistry B, 2017, 121, 3586-3596.	2.6	17
76	Accelerating electron tomography reconstruction algorithm ICON with GPU. Biophysics Reports, 2017, 3, 36-42.	0.8	17
77	Structure-based evidence for the enhanced transmissibility of the dominant SARS-CoV-2 B.1.1.7 variant (Alpha). Cell Discovery, 2021, 7, 109.	6.7	17
78	AuTom-dualx: a toolkit for fully automatic fiducial marker-based alignment of dual-axis tilt series with simultaneous reconstruction. Bioinformatics, 2019, 35, 319-328.	4.1	15
79	New interfaces on MiD51 for Drp1 recruitment and regulation. PLoS ONE, 2019, 14, e0211459.	2.5	15
80	VHUT-cryo-FIB, a method to fabricate frozen hydrated lamellae from tissue specimens for in situ cryo-electron tomography. Journal of Structural Biology, 2021, 213, 107763.	2.8	15
81	Single-particle reconstruction using L2-gradient flow. Journal of Structural Biology, 2011, 176, 259-267.	2.8	14
82	Determining the target protein localization in 3D using the combination of FIB-SEM and APEX2. Biophysics Reports, 2017, 3, 92-99.	0.8	14
83	Orienting the future of bio-macromolecular electron microscopy. Chinese Physics B, 2018, 27, 063601.	1.4	14
84	SmartBac, a new baculovirus system for large protein complex production. Journal of Structural Biology: X, 2019, 1, 100003.	1.3	14
85	Flexible interwoven termini determine the thermal stability of thermosomes. Protein and Cell, 2013, 4, 432-444.	11.0	13
86	A local-optimization refinement algorithm in single particle analysis for macromolecular complex with multiple rigid modules. Protein and Cell, 2016, 7, 46-62.	11.0	13
87	Imaging biological samples by integrated differential phase contrast (iDPC) STEM technique. Journal of Structural Biology, 2022, 214, 107837.	2.8	13
88	Cryo-EM structure and electrophysiological characterization of ALMT from <i>Glycine max</i> reveal a previously uncharacterized class of anion channels. Science Advances, 2022, 8, eabm3238.	10.3	13
89	Structural characterization of coatomer in its cytosolic state. Protein and Cell, 2016, 7, 586-600.	11.0	12
90	Using integrated correlative cryo-light and electron microscopy to directly observe syntaphilin-immobilized neuronal mitochondria in situ. Biophysics Reports, 2017, 3, 8-16.	0.8	12

#	Article	IF	CITATIONS
91	The late stage of COPI vesicle fission requires shorter forms of phosphatidic acid and diacylglycerol. Nature Communications, 2019, 10, 3409.	12.8	11
92	A 3.3â€Ãâ€Resolution Structure of Hyperthermophilic Respiratory Complexâ€III Reveals the Mechanism of It Thermal Stability. Angewandte Chemie - International Edition, 2020, 59, 343-351.	^{TS} 13.8	11
93	Structural insights into membrane remodeling by SNX1. Proceedings of the National Academy of Sciences of the United States of America, 2021, 118, .	7.1	11
94	Preliminary molecular characterization and crystallization of mitochondrial respiratory complex II from porcine heart. FEBS Journal, 2007, 274, 1524-1529.	4.7	10
95	Expression, purification and preliminary biochemical studies of the N-terminal domain of leucine-rich repeat kinase 2. Biochimica Et Biophysica Acta - Proteins and Proteomics, 2010, 1804, 1780-1784.	2.3	10
96	Dimerization Interface of 3-Hydroxyacyl-CoA Dehydrogenase Tunes the Formation of Its Catalytic Intermediate. PLoS ONE, 2014, 9, e95965.	2.5	10
97	Structural Insight into the Specific DNA Template Binding to DnaG primase in Bacteria. Scientific Reports, 2017, 7, 659.	3.3	10
98	Cryo-EM structures of the air-oxidized and dithionite-reduced photosynthetic alternative complex III from <i>Roseiflexus castenholzii</i> . Science Advances, 2020, 6, eaba2739.	10.3	10
99	Distinct symmetry and limited peptide refolding activity of the thermosomes from the acidothermophilic archaea Acidianus tengchongensis S5T. Biochemical and Biophysical Research Communications, 2010, 393, 228-234.	2.1	9
100	BrkAutoDisplay: functional display of multiple exogenous proteins on the surface of Escherichia coli by using BrkA autotransporter. Microbial Cell Factories, 2015, 14, 129.	4.0	9
101	Crystal structure of the N-terminal SH3 domain of mouse βPIX, p21-activated kinase-interacting exchange factor. Biochemical and Biophysical Research Communications, 2006, 339, 407-414.	2.1	8
102	Purification, crystallization and preliminary crystallographic analysis of very-long-chain acyl-CoA dehydrogenase fromCaenorhabditis elegans. Acta Crystallographica Section F: Structural Biology Communications, 2010, 66, 426-430.	0.7	7
103	Identification of neurons responsible for feeding behavior in the Drosophila brain. Science China Life Sciences, 2014, 57, 391-402.	4.9	7
104	Isolated Heme A Synthase from Aquifex aeolicus Is a Trimer. MBio, 2020, 11, .	4.1	6
105	Molecular mechanism of mitochondrial phosphatidate transfer by Ups1. Communications Biology, 2020, 3, 468.	4.4	6
106	Cellular 3D-reconstruction and analysis in the human cerebral cortex using automatic serial sections. Communications Biology, 2021, 4, 1030.	4.4	6
107	Expression, purification, crystallization and crystallographic study of the <i>Aspergillus terreus</i> aromatic prenyltransferase AtaPT. Acta Crystallographica Section F, Structural Biology Communications, 2015, 71, 889-894.	0.8	5
108	The Unusual Homodimer of a Hemeâ€Copper Terminal Oxidase Allows Itself to Utilize Two Electron Donors. Angewandte Chemie - International Edition, 2021, 60, 13323-13330.	13.8	5

#	Article	IF	CITATIONS
109	Crystallization and preliminary X-ray analysis of recombinant histone HPhA from the hyperthermophilic archaeonPyrococcus horikoshiiOT3. Acta Crystallographica Section D: Biological Crystallography, 2002, 58, 870-871.	2.5	4
110	A fast calculation strategy of density function in ISAF reconstruction algorithm. Science China Information Sciences, 2013, 56, 1-12.	4.3	4
111	Expression, purification and preliminary characterization of glucagon receptor extracellular domain. Protein Expression and Purification, 2013, 89, 232-240.	1.3	4
112	A 3.3â€Ââ€Resolution Structure of Hyperthermophilic Respiratory Complexâ€III Reveals the Mechanism of It Thermal Stability. Angewandte Chemie, 2020, 132, 351-359.	^s 2.0	4
113	Prokaryotic Expression of Active Mitochondrial Uncoupling Protein 1*. Progress in Biochemistry and Biophysics, 2010, 37, 56-62.	0.3	4
114	Puzzle out the regulation mechanism of PI4KIIα activity. Science China Life Sciences, 2014, 57, 636-638.	4.9	3
115	ICON-MIC: Implementing a CPU/MIC Collaboration Parallel Framework for ICON on Tianhe-2 Supercomputer. Journal of Computational Biology, 2018, 25, 270-281.	1.6	3
116	Reprint of "Amorphous nickel titanium alloy film: A new choice for cryo electron microscopy sample preparation― Progress in Biophysics and Molecular Biology, 2021, 160, 5-15.	2.9	3
117	D Structural Investigation of Caveolae From Porcine Aorta Endothelial Cell by Electron Tomography*. Progress in Biochemistry and Biophysics, 2009, 2009, 729-735.	0.3	3
118	Developing Graphene Grids for Cryoelectron Microscopy. Frontiers in Molecular Biosciences, 0, 9, .	3.5	3
119	Expression, crystallization and preliminary X-ray studies of the recombinant PTB domain of mouse dok1 protein. Acta Crystallographica Section D: Biological Crystallography, 2004, 60, 334-336.	2.5	2
120	Three-dimensional visualization of arsenic stimulated mouse liver sinusoidal by FIB-SEM approach. Protein and Cell, 2016, 7, 227-232.	11.0	2
121	ACAP1 assembles into an unusual protein lattice for membrane deformation through multiple stages. PLoS Computational Biology, 2019, 15, e1007081.	3.2	2
122	Purification, crystallization and preliminary crystallographic analysis of 3-hydroxyacyl-CoA dehydrogenase fromCaenorhabditis elegans. Acta Crystallographica Section F: Structural Biology Communications, 2013, 69, 515-519.	0.7	1
123	Expression, purification, crystallization and preliminary crystallographic study of the cytoplasmic domain of the mitochondrial dynamics protein MiD51. Acta Crystallographica Section F, Structural Biology Communications, 2014, 70, 596-599.	0.8	1
124	C-terminal motif within Sec7 domain regulates guanine nucleotide exchange activity via tuning protein conformation. Biochemical and Biophysical Research Communications, 2014, 446, 380-386.	2.1	1
125	Autogdeterm: automatic geometry determination for electron tomography. Tsinghua Science and Technology, 2018, 23, 369-376.	6.1	1
126	A Fully Automatic Geometric Parameters Determining Method for Electron Tomography. Lecture Notes in Computer Science, 2017, , 385-389.	1.3	1

#	Article	IF	CITATIONS
127	Site-Directed Mutagenesis and Preliminary X-Ray Crystallographic Studies of the Tabtoxin Resistance Protein. Protein and Peptide Letters, 2003, 10, 255-263.	0.9	1
128	Substrate Binding Properties of Thermosome ATcpnβFrom <i>Acidianus Tengchongensis</i> . Progress in Biochemistry and Biophysics, 2011, 38, 151-158.	0.3	1
129	Research of Mitochondrial Calcium Transportation. Sheng Wu Wu Li Hsueh Bao, 2013, 29, 167.	0.1	1
130	Accelerating Electron Tomography Reconstruction Algorithm ICON Using the Intel Xeon Phi Coprocessor on Tianhe-2 Supercomputer. Lecture Notes in Computer Science, 2017, , 258-269.	1.3	1
131	A fast mapping method in the ISAF reconstruction algorithm. , 2011, 2011, 3930-3.		0
132	Interference microscopy volume illustration for biomedical data. , 2012, , .		0
133	Fabrication of Frozen-Hydrated Sections by Focused Ion Beam(FIB) Method. Microscopy and Microanalysis, 2016, 22, 182-183.	0.4	0
134	Editorial overview: New insights into membrane protein machineries from technology revolution. Current Opinion in Structural Biology, 2020, 63, iii-v.	5.7	0
135	Frontispiz: A 3.3â€Ãâ€Resolution Structure of Hyperthermophilic Respiratory Complexâ€III Reveals the Mechanism of Its Thermal Stability. Angewandte Chemie, 2020, 132, .	2.0	0
136	Frontispiece: A 3.3â€Ãâ€Resolution Structure of Hyperthermophilic Respiratory Complexâ€III Reveals the Mechanism of Its Thermal Stability. Angewandte Chemie - International Edition, 2020, 59, .	13.8	0
137	The Unusual Homodimer of a Hemeâ€Copper Terminal Oxidase Allows Itself to Utilize Two Electron Donors. Angewandte Chemie, 2021, 133, 13435-13442.	2.0	0
138	Electron Microscopy Reconstruction of Helical Assemblies. Sheng Wu Wu Li Hsueh Bao, 2013, 29, 879.	0.1	0